

SANDIA REPORT

SAND2006-7842

Unlimited Release

Printed January 2007

LDRD Final Report on High Power Broadly Tunable Mid-IR Quantum Cascade Lasers for Improved Chemical Species Detection

Erik W. Young, Michael C. Wanke, John F. Klem, Charles T. Fuller,
Sally Samora, and James J. Hudgens

Prepared by
Sandia National Laboratories
Albuquerque, New Mexico 87185 and Livermore, California 94550

Sandia is a multiprogram laboratory operated by Sandia Corporation,
a Lockheed Martin Company, for the United States Department of Energy's
National Nuclear Security Administration under Contract DE-AC04-94AL85000.

Approved for public release; further dissemination unlimited.



Sandia National Laboratories

Issued by Sandia National Laboratories, operated for the United States Department of Energy by Sandia Corporation.

NOTICE: This report was prepared as an account of work sponsored by an agency of the United States Government. Neither the United States Government, nor any agency thereof, nor any of their employees, nor any of their contractors, subcontractors, or their employees, make any warranty, express or implied, or assume any legal liability or responsibility for the accuracy, completeness, or usefulness of any information, apparatus, product, or process disclosed, or represent that its use would not infringe privately owned rights. Reference herein to any specific commercial product, process, or service by trade name, trademark, manufacturer, or otherwise, does not necessarily constitute or imply its endorsement, recommendation, or favoring by the United States Government, any agency thereof, or any of their contractors or subcontractors. The views and opinions expressed herein do not necessarily state or reflect those of the United States Government, any agency thereof, or any of their contractors.

Printed in the United States of America. This report has been reproduced directly from the best available copy.

Available to DOE and DOE contractors from

U.S. Department of Energy
Office of Scientific and Technical Information
P.O. Box 62
Oak Ridge, TN 37831

Telephone: (865) 576-8401
Facsimile: (865) 576-5728
E-Mail: reports@adonis.osti.gov
Online ordering: <http://www.osti.gov/bridge>

Available to the public from

U.S. Department of Commerce
National Technical Information Service
5285 Port Royal Rd.
Springfield, VA 22161

Telephone: (800) 553-6847
Facsimile: (703) 605-6900
E-Mail: orders@ntis.fedworld.gov
Online order: <http://www.ntis.gov/help/ordermethods.asp?loc=7-4-0#online>



SAND2006-7842
Unlimited Release
Printed January 2007

LDRD Final Report on High Power Broadly Tunable Mid-IR Quantum Cascade Lasers for Improved Chemical Species Detection

Erik W. Young, Michael C. Wanke, Charles T. Fuller,
Sally Samora, and James J. Hudgens
Photonic Microsystems Technologies Department

John F. Klem
RF/Optoelectronics Department

Sandia National Laboratories
P.O. Box 5800
Albuquerque, New Mexico 87185-MS1082

Abstract

The goal of our project was to examine a novel quantum cascade laser design that should inherently increase the output power of the laser while simultaneously providing a broad tuning range. Such a laser source enables multiple chemical species identification with a single laser and/or very broad frequency coverage with a small number of different lasers, thus reducing the size and cost of laser based chemical detection systems. In our design concept, the discrete states in quantum cascade lasers are replaced by minibands made of multiple closely spaced electron levels. To facilitate the arduous task of designing miniband-to-miniband quantum cascade lasers, we developed a program that works in conjunction with our existing modeling software to completely automate the design process. Laser designs were grown, characterized, and iterated. The details of the automated design program and the measurement results are summarized in this report.

ACKNOWLEDGMENTS

The authors would like to acknowledge the help of Deborah Sivco of Lucent Technologies for materials growth. We also wish to thank Dan Wasserman of Princeton University for help with processing and characterization of the laser samples.

TABLE OF CONTENTS

Abstract	3
Acknowledgments.....	4
Table of Contents	5
List of Figures.....	6
Nomenclature.....	7
1. Introduction.....	9
2. Automated Design Program.....	11
2.1. Design Parameters	12
2.2. First Well.....	15
2.3. Active Region.....	15
2.4. Injector	17
2.5. Final Barrier and Field Feedback	17
2.6. Finished Design.....	19
3. Measurements	25
3.1. First growth.....	25
3.2. Second growth.....	27
4. Conclusions.....	33
Appendix A: Program Code	35
Distribution.....	42

LIST OF FIGURES

Figure 1: Optical transition shown in red occurs between two discrete states in A, and two wide minibands in B.....	10
Figure 2: Schematic showing the fundamentals of quantum cascade laser structures.....	12
Figure 3: Perfectly aligned 4-level miniband.	13
Figure 4: Slightly misaligned 4-level miniband.	13
Figure 5: Perfectly aligned 6-level miniband.	14
Figure 6: Slightly misaligned 6-level miniband.	14
Figure 7: Example of the effect of the central barrier thickness on the energy level and shape of the modulus squared wavefunctions of the lowest two energy levels in the well. The energy levels are color-matched to the barrier that created them.	16
Figure 8: Flowchart of the design process for the active region.....	18
Figure 9: The finished broad gain QCL design.	20
Figure 10: Expanded view of the first (and fourth) miniband in the laser design.	20
Figure 11: Expanded view of the second miniband in the laser design.	21
Figure 12: Expanded view of the third miniband in the laser design.	21
Figure 13: Expanded view of the lasing transition in the laser design.....	22
Figure 14: Expanded view of the first phonon drop in the laser design.....	23
Figure 15: Expanded view of the second phonon drop in the laser design.	23
Figure 16: Partly processed sample of D3224 showing the large number of defects. The central waveguide is 24 microns wide.	25
Figure 17: An unprocessed sample of D3234 showing the high defect density.....	26
Figure 18: Representative current-voltage plot of laser bars from wafer D3224.	27
Figure 19: Comparison of current-voltage curves for laser bars from EB2569 and D3224.	28
Figure 20: Current-voltage curves at T = 4K for two LED's fabricated from wafer EB2569.....	28
Figure 21: Current-voltage curves at T = 294K for LED's fabricated from wafer EB2571.....	29
Figure 22: Current-voltage curves at T=4K and T=300K for an LED from wafer EB2555.....	29
Figure 23: Degradation of the current-voltage curve over time of and LED from wafer EB2555.....	31
Figure 24: Spectrum of lasing sample from EB2569.....	31
Figure 25: Spectrum of light emission from EB2571.	32

NOMENCLATURE

DOE	Department of Energy
I-V	Current-Voltage
LDRD	Lab Directed Research and Development
LO	Longitudinal-Optical
QC	Quantum Cascade
QCL	Quantum Cascade Laser
SNL	Sandia National Laboratories

1. INTRODUCTION

Mid-infrared quantum cascade lasers can be used for large stand-off remote sensing of a variety of chemical species of special interest to national security. While demonstrations have proved that individual molecular species can be remotely identified using quantum cascade lasers, the lasers are generally designed for a specific wavelength of operation with a narrow window over which they can be tuned. Thus, identification of multiple species requires multiple laser sources, each with a different design.

Tunable quantum cascade lasers would improve chemical species detection systems. The ability to detect multiple chemical species using a single laser source instead of multiple laser sources reduces both the size and cost of the detection system. However, though a few others have demonstrated broadly tunable QC lasers, existing designs inherently sacrifice power for tunability. This reduction in output power limits the range and effectiveness of these tunable lasers in stand-off remote chemical species detection.

The goal of our project was to examine a novel quantum cascade laser design that should inherently increase the output power of the laser while providing a broad tuning range. This enables multiple chemical species identification with a single laser and/or very broad frequency coverage with a small number of different lasers, thus reducing the size and cost of chemical detection systems. Commonly, the lasing transition in a quantum cascade laser is an intraband transition between two discrete electron levels (Figure 1a). In our design concept, the discrete states are replaced by minibands made of multiple closely spaced electron levels (Figure 1b).

Several approaches have been used to realize broad gain quantum cascade lasers including electrical tuning of a diagonal transition [Muller et al., *Appl. Phys. Lett.*, 75, 1509 (1999)], using a chirped superlattice [Gmachl et al., *Nature*, 415, 883 (2002)], and bound to continuum transitions [Maulini et al., *Appl. Phys. Lett.*, 84, 1659 (2004)]. Previous and ongoing approaches to obtaining high power broadly tunable quantum cascade lasers have limitations to their output powers and tuning ranges, which should be overcome by our design. Electrically tuning a diagonal transition limits the tuning range and has a weaker dipole moment, reducing the output power. Very broad gain has been achieved using a chirped superlattice composed of many quantum wells, each designed to lase at a separate wavelength. However, this design results in low power for any given wavelength within the bandwidth and is highly inefficient spectrally. Bound to continuum transitions are similar in principle to our design in that their lower isolated electron level is replaced with a miniband. However, the use of an isolated upper electron level limits current flow and output power, as well as the tuning range.

In our design, the minibands provide a wide tuning range. The wavefunctions in the minibands are closely coupled to each other. As long as the total energy width of the miniband does not exceed the typical linewidth of the optical transition of the isolated level case, then the electrons in any state in the miniband can be coerced into emitting a wavelength chosen by a separate tuning mechanism, e.g. an external grating. The tuning range is bounded by the energy difference between the top of the upper miniband and the bottom of the lower miniband to the energy difference between the bottom of the upper miniband and the top of the lower miniband.

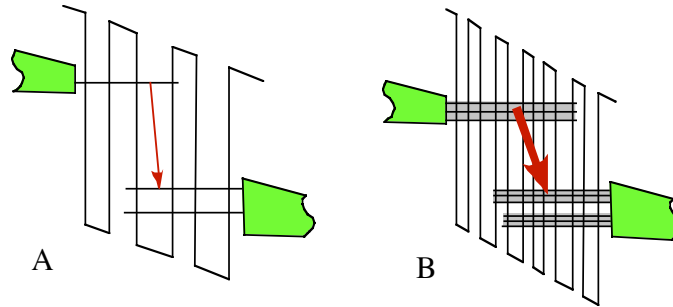


Figure 1: Optical transition shown in red occurs between two discrete states in A, and two wide minibands in B.

Given the typical parameters in a 10 micron quantum cascade laser, the bandwidth of the laser gain can be greater than 10% of the center frequency.

In addition to providing broad gain without sacrificing power, the minibands should improve the performance of the lasers. Quantum cascade lasers are made up of stacks of thin quantum wells and rely on tunneling for carrier transport. Increasing the number of available states to tunnel into via a miniband lowers the device resistance and increases the current carrying capability of the laser. This higher current capacity enables higher optical power output, while the overall efficiency of the laser increases due to the lower resistance.

To facilitate the design of these complex structures, we also proposed to incorporate into our existing modeling software, which we have been developing for the past four years, new code that will automate calculation of quantum cascade miniband structures based on predetermined design rules and desired parameters. The typical design process for quantum cascade lasers involves numerous iterations between choosing an applied electric field, designing the layers of the structure, then calculating what the field should be. Increasing the number of electron levels increases the complexity of designing the quantum cascade structure, as the wavefunctions must align appropriately at the same applied electric field. In addition, the width of the minibands, spacing between minibands, and proper coupling strengths between wells must be realized at this same field. The proposed design software reduces the turnaround time between design iterations and improves consistency between designs for our structure, as well as provides enhanced, quick, and economical designs of a variety of other quantum cascade lasers.

2. AUTOMATED DESIGN PROGRAM

The most crucial element of the project is the design of the quantum cascade laser structure. A schematic illustrating the fundamentals of a quantum cascade laser structure is shown in Figure 2. Quantum cascade lasers are intraband lasers, where lasing occurs due to electrons losing energy as they transition between states or minibands in the conduction band. The region of the structure where the lasing transition is located is called the active region. The injector is the portion of the structure that “injects” electrons into the upper level of the active region. Together, the injector and active region make up a unit cell or stage. The stages are repeated back to back many times in a single structure to allow for recycling of the electron by making the electrons leaving one stage equal to the input for the next stage. Hence the “cascade” in quantum cascade laser. Thus, the injector not only injects electrons into the active region, but also extracts electrons from the previous active region. In our design, this is done with the designed emission of two longitudinal-optical (LO) phonons, which have fast transitions. It is necessary to have a faster rate of extraction than the rate of radiative transition in order to achieve population inversion, and thus lasing.

Great care must be taken to ensure that each well and each barrier are the correct width in order to get proper band lineups from well to well. The problem is magnified in the broad gain lasers, as the design relies on transitions between minibands instead of single states. Each miniband must be designed such that not only is there adequate coupling between all of the levels in each miniband (the tightness of the bands), but that there is also a proper distribution of the wavefunctions in the minibands to allow efficient transitions. Misalignment of the bands can prevent certain energy transitions, causing holes in the tuning range or preventing efficient current flow. Figures 3-6 illustrate the differences in perfectly aligned and misaligned minibands for 4 and 6 level cases.

To facilitate the design of these complex structures, we successfully incorporated into our existing modeling software new code that automates the calculation of quantum cascade miniband structures based on predetermined design rules and desired parameters (Appendix A). The typical design process for quantum cascade lasers involves numerous iterations between choosing an applied electric field, designing the layers of the structure, then calculating what the field should be. Increasing the number of electron levels increases the complexity of designing the quantum cascade structure, as the wavefunctions must align appropriately at the same applied electric field. In addition, the width of the minibands, spacing between minibands, and proper coupling strengths between wells must be realized at this same field. Our automated design software provides us the ability to quickly and efficiently produce and iterate quantum cascade laser designs. The software improves consistency between designs for our structure, as well as provides enhanced, quick, and economical designs of a variety of other quantum cascade lasers.

The new design program is written for Matlab as an m-file. The program repeatedly calls our existing modeling software, which is written in C, each time sending a new structure file to be processed. The results of the modeling software are then evaluated and the design software decides what modifications to make to the structure file. The functionality of the program will be discussed in the following sections.

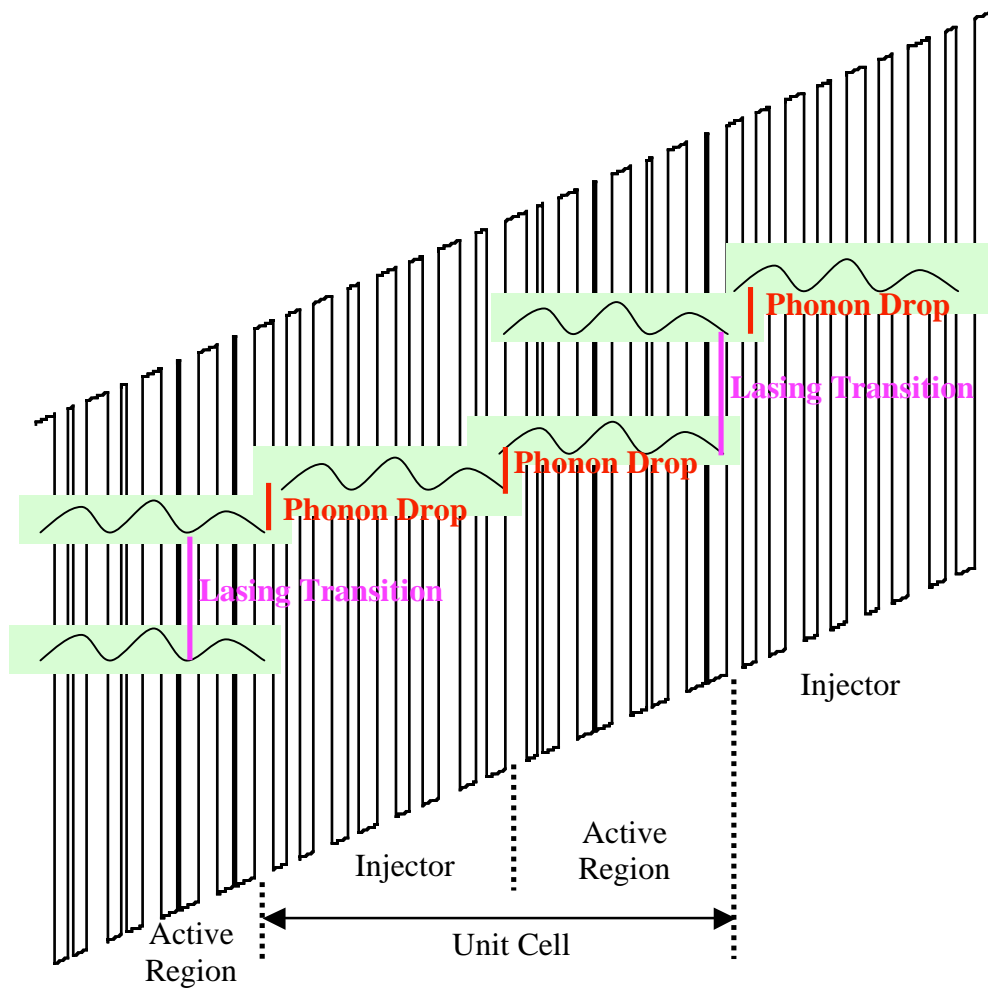


Figure 2: Schematic showing the fundamentals of quantum cascade laser structures.

2.1. Design Parameters

For the lasers investigated in this project, the design wavelength was targeted to be 10 microns. This roughly corresponds to an energy transition of 120 meV. A common practice in quantum cascade lasers designs is to incorporate LO phonon drops below the lower energy level of the lasing transition. This promotes population inversion, as the phonon drop has a fast transition rate while the rate for the lasing transition is much slower. In our design, we decided to incorporate two phonon drops, each equal to the LO phonon energy of approximately 36 meV.

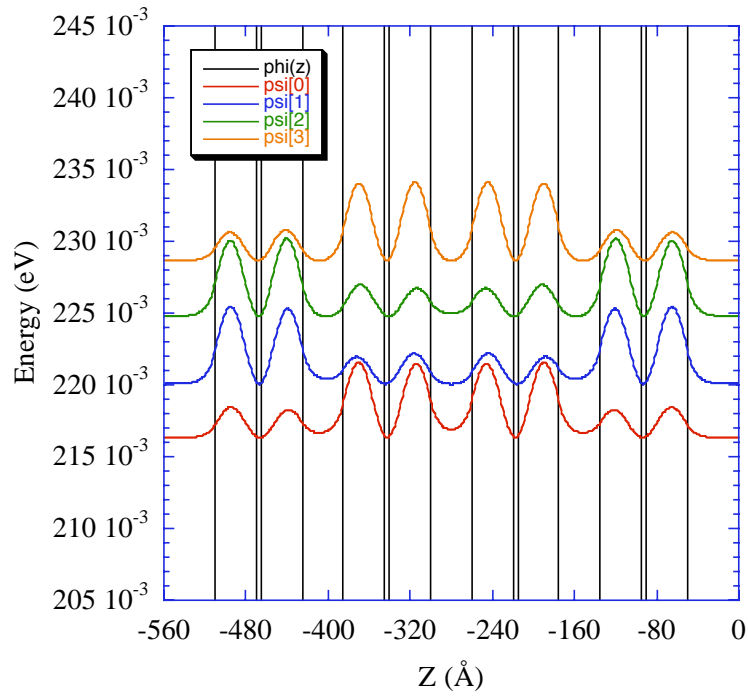


Figure 3: Perfectly aligned 4-level miniband.

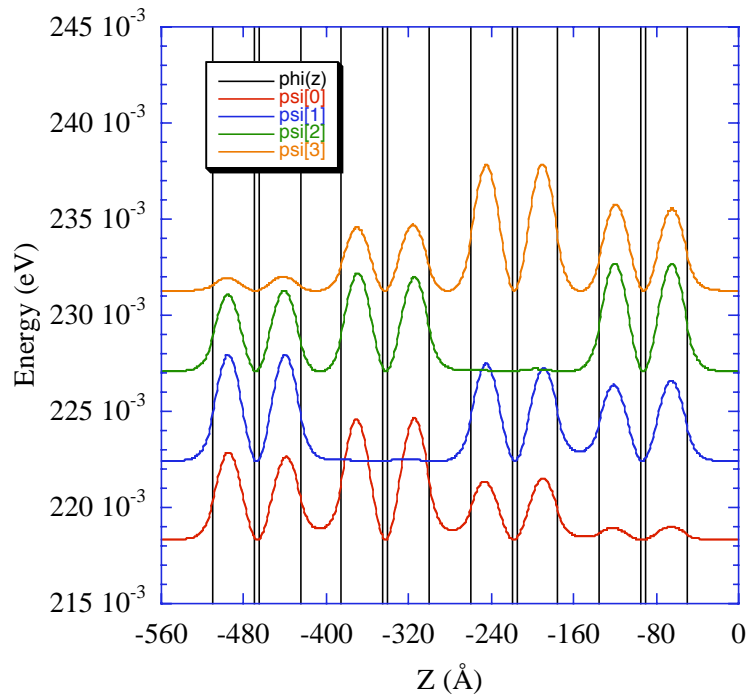


Figure 4: Slightly misaligned 4-level miniband.

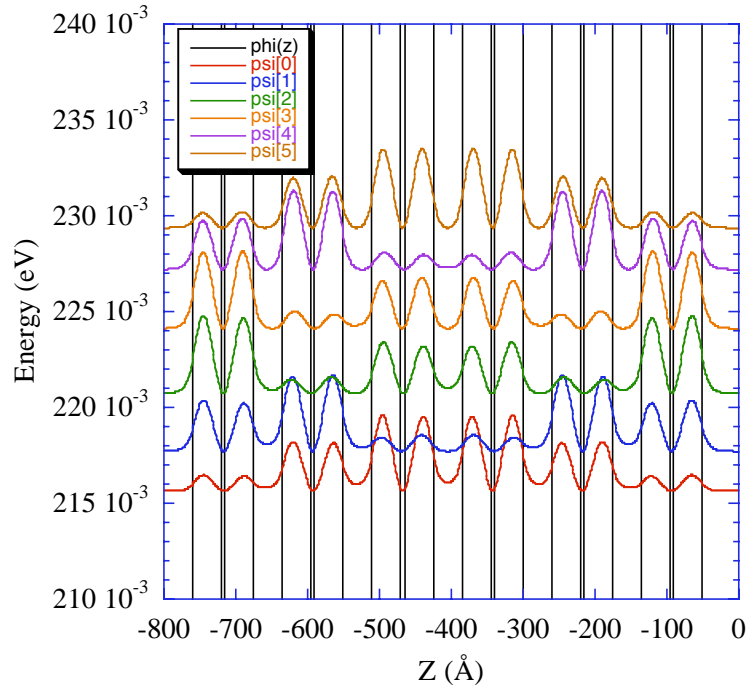


Figure 5: Perfectly aligned 6-level miniband.

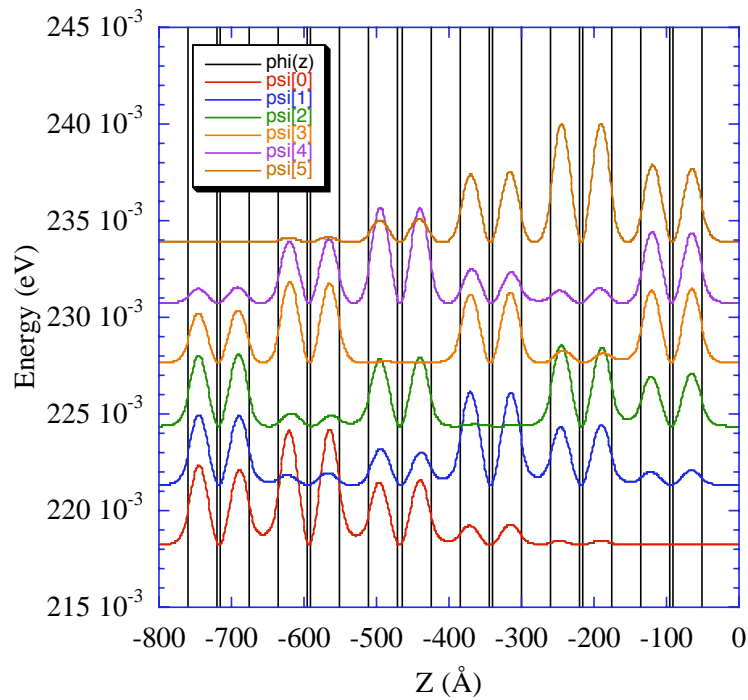


Figure 6: Slightly misaligned 6-level miniband.

There are many parameters that must be chosen such as band drops, band splittings, and associated tolerances. These will be defined and discussed in more detail in the following sections. However, the most important input parameter is the applied electric field. All well and barrier widths will be affected by this parameter. Proper choice of the field will reduce the computation time. However, any choice will eventually lead to a solution, as the program recalculates what the field should be after each iteration, and continues to run until the proper field is found that matches all of the other design criteria.

2.2. First Well

The easiest part of the program is the design of the first well. In reality, all “wells” in the program are bi-wells, i.e. pairs of wells with a thin barrier in them. The thickness and position of this central barrier affects the position and distribution of the energy levels in the well, as illustrated in Figure 7. When the barrier is thin and is located in the middle of the well, the perturbation on the lower wavefunction is strong, since the first-order wavefunction peaks in the middle of the well. The second-order wavefunction has a trough in the middle of the well. Thus, perturbations to the second-order wavefunction are small under these conditions. Increasing the size of the barrier and/or moving the barrier away from the center of the well will change the locations of the two energy levels.

The user selects the desired bandgap (the energy separation between the lowest two energy levels), which for our design is 120 meV. The thickness of the central barrier is also chosen. In our design, this initial barrier thickness was chosen to match the lattice constant of InP. Given the applied electric field, the program iterates between varying the thickness of the well to match the bandgap within a given tolerance and varying the location of the central barrier to align the wavefunctions in both halves of the well with each other. This latter is equivalent to saying that the lowest state in each well of the pair is maximally coupled (or anti-crossed) with the state in the opposite well.

2.3. Active Region

Our quantum cascade laser design relies on an energy transition between two minibands rather than two discrete states. Therefore, the next step is to create more wells whose top (level 2) and bottom (level 1) states line up with the states from the first well at the applied electric field. This set of wells is referred to as the active region. Due to the necessary presence of the electric field the bottoms of neighboring wells do not line up, but drop in the direction of current flow. Therefore, since the energy levels relative to the bottom of the wells depend on the well width, the new wells cannot simply be duplicates of the first well. The states would not line up properly, with the energy levels of the new well being below the energy levels of the previous well. Thus, each additional well must be narrowed to push the state higher as the bottom of the well drops. A collection of wells, where each well is narrower than the previous to provide alignment of the states at some finite electric field, is referred to as a chirped superlattice.

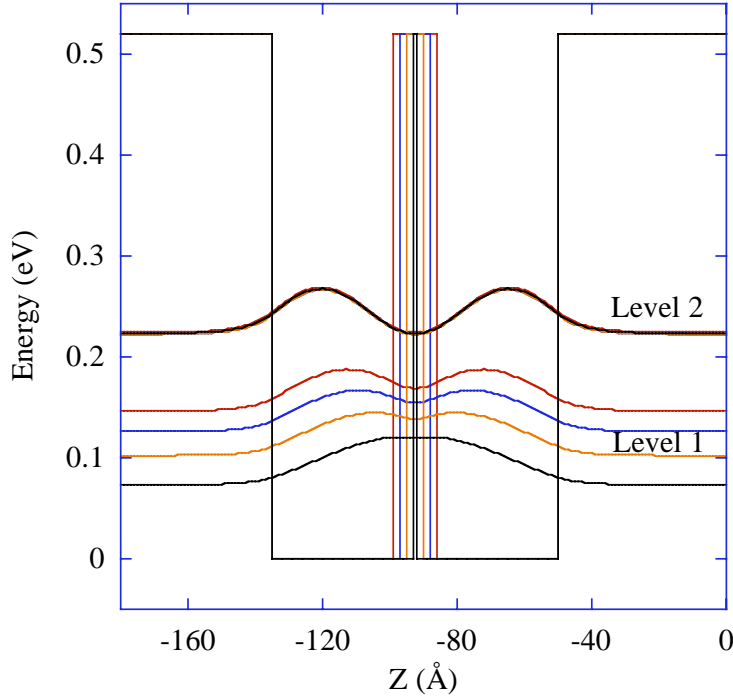


Figure 7: Example of the effect of the central barrier thickness on the energy level and shape of the modulus squared wavefunctions of the lowest two energy levels in the well. The energy levels are color-matched to the barrier that created them.

For these designs, we are trying to line up two levels simultaneously in the presence of an electric field. This requires more degrees of freedom than possible with just changing the well width as in simple chirped superlattices. Thus, we use bi-wells, where we can control the first two levels independently. To do so the well width is made narrower to raise level 2, while the central barrier is broadened to raise level 1. The thickness of the barrier between the bi-wells also must be designed. This thickness controls the amount of coupling between neighboring bi-wells. The thinner this thickness, the more coupling there will be. However, as the coupling increases, so does the splitting of the aligned bands in an energy level, which increases the width of the miniband. The energy separation between individual states in the minibands needs to remain small enough so that the total energy width of the miniband does not exceed the typical linewidth of the optical transition of the isolated level case, in order to allow electrons to populate any state in the miniband and thus achieve broad gain with high power.

When creating the active region, the program only looks at two bi-wells at a time: the new bi-well and the previous bi-well. The program attempts to line up the energy level of the two wells while achieving a defined energy splitting between the upper energy levels of the two wells. Iteration of a nested loop is needed in order to properly meet all of the design criteria.

In the inner loop, the value of the separation barrier is determined. First, the upper energy level of the two wells is matched by changing the new well width. The values of the energy levels are not compared, as they will not be equal due to the designed splitting between them. Rather, the distributions of the wavefunctions in each bi-well are compared. The two energy levels are aligned when each wavefunction exhibits the same weight on each side of the separation barrier as the other wavefunction. The desired energy splitting between these two states is then reached by varying the separation barrier width.

The outer loop then continues to align the energy levels. The upper energy levels are aligned as explained above. The lower energy levels are aligned in a similar fashion, where the width of the new well's central barrier is used to achieve proper alignment. The position of the thin central barrier in the well is then varied to better align the wavefunctions. The loops are iterated until the design criteria for upper and lower band alignments and band splittings are met. A flowchart of the design process for the active region is shown in Figure 8.

2.4. Injector

The injector consists of two LO phonon drops, each 36 meV. Again, our design substitutes minibands for discrete states. This theoretically allows for a larger current flow through decreased resistance. The injector region consists of four bi-wells. The first well provides a phonon drop, while the second well creates a miniband with the first. The second phonon drop and miniband are provided by the third and fourth wells, respectively.

The program creates the injector in a similar fashion to the active region by only comparing two neighboring wells at a time. Therefore, the first injector well is compared to the last well in the active region. To incorporate the phonon drop, state 2 of the injector well must be aligned to state 1 of the active region well. The second injector well is matched to the first, with state 2 from the second well aligned to state 2 of the first well. The second phonon drop requires state 2 of the third well to align with state 1 of the second well. The fourth well is then matched to the third well, with both state 1 and state 2 aligned between the wells.

2.5. Final Barrier and Field Feedback

The “cascade” in quantum cascade laser comes from using a single electron to emit many photons by sending the electron through many identical energy drops. This is achieved by repeating the unit cell over and over (in our design, 20 times). Thus, state 1 of the last well in the unit cell (injector well 4) must match up with state 2 in the first well of the unit cell (active region well 1). The energy levels must also have the proper coupling between them.

Our program first tackles the coupling issue. The first well of the active region is compared to the last well of the injector. The width of the barrier between them is then iterated until the proper energy splitting between the levels is achieved. Controls are put in place to prevent endless loops, as not all design conditions can be met for a given electric field. The final barrier width can even be negative if the specified design field is far from the optimum value.

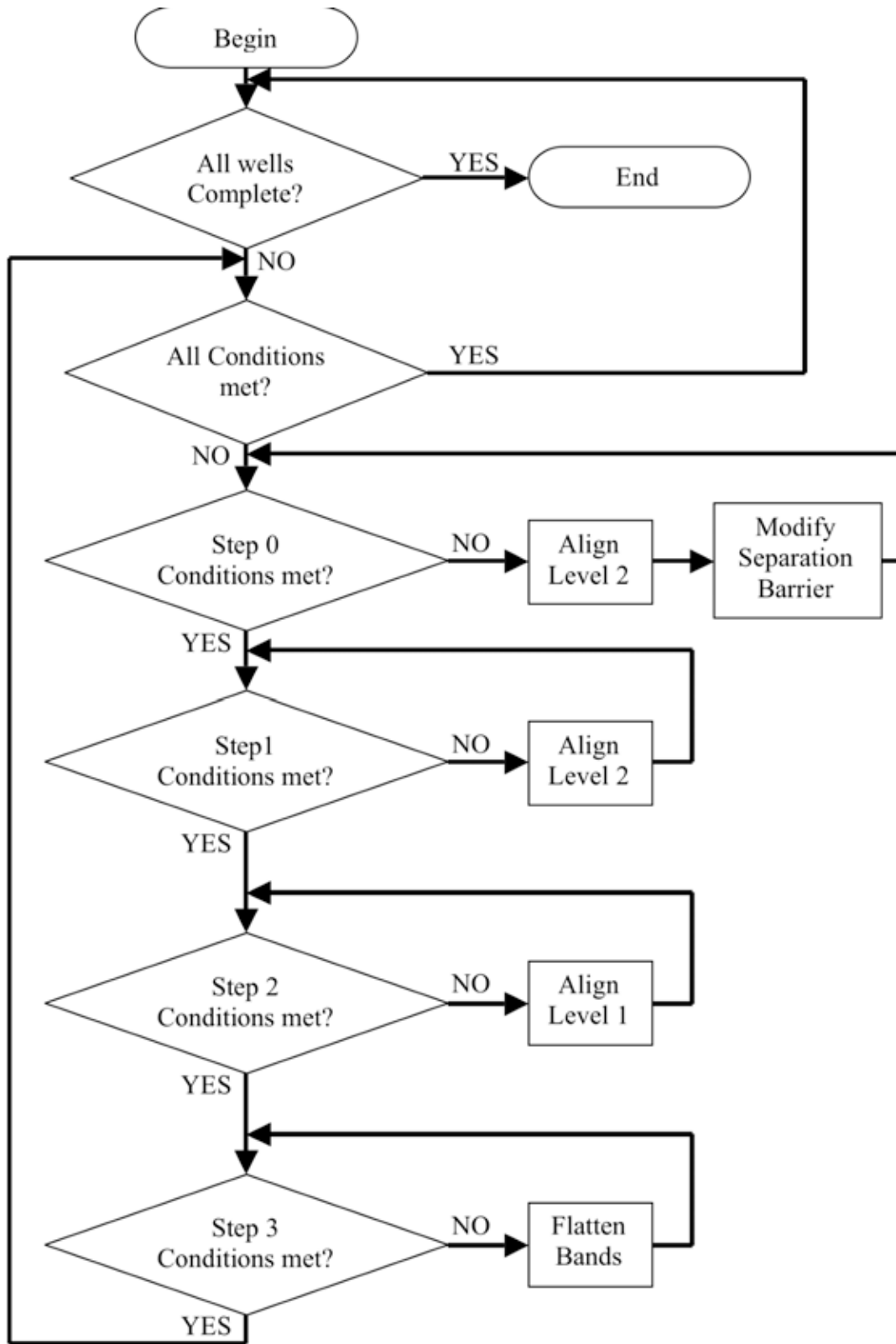


Figure 8: Flowchart of the design process for the active region.

Once the final barrier width is determined, the voltage drop across the unit cell is calculated from the applied electric field and the total unit cell thickness. This voltage drop is then compared to the average voltage drop between the highest and lowest minibands, approximately 192 meV in our design. If the voltage drops do not match within a given tolerance, a new electric field is calculated based on the previous design, and the program starts again.

2.6. Finished Design

The finished design for the broad gain quantum cascade laser is shown in Figure 9. More than one unit cell is plotted to show all of the band lineups. Expanded views of the first three minibands are shown in Figures 10-12. The fourth miniband in Figure 9 is the same as the first miniband.

The quality of these minibands can be determined from Figures 3-6. The first miniband (Figure 10) shows very good agreement with the perfect 6-level case of Figure 5. However, all of the wavefunctions are shifted slightly to the left. In fact, the first miniband almost perfectly matches a 5-level case, with $\psi[2]$ and $\psi[3]$ acting as a single level. The bottom four levels of the second miniband (Figure 11) show very good agreement with Figure 5. However, the top two levels of the second miniband are shifted to the left, $\psi[5]$ more so than $\psi[4]$. The third miniband (Figure 12) is slightly misaligned, looking more similar to Figure 4 than to Figure 3.

There are several reasons why the designed minibands do not match the perfect cases. Part of the problem is the way the minibands are designed. When creating the structure, we look at only two wells at a time. The boundaries beyond these wells are barriers with infinite thickness. However, in real life the defining barriers have a finite thickness; thus, the confinement will be less than what was designed for. Another problem is the phonon drops. These drops require the matching of the level 1's from one set of wells to the level 2's of another set of wells. This can only be accomplished through a large variation in both the well and barrier widths, as can be seen on the right hand side of Figure 10 and the left hand side of Figure 11. These larger barriers as compared to the active region make it harder to couple the wavefunctions equally between all wells in the miniband, resulting in shifts of the wavefunctions. In the case of the first miniband, the large separation barrier for the rightmost well nearly isolates this well from the rest of the miniband, resulting in a quasi-5-level miniband. Also, the wavefunction symmetry is different for ground states and first excited states. Another problem is due to the cyclical, cascading nature of the design where the last level must line up to the first. This required the energy splittings of the upper states in the injector wells to go from tight to loose in order to match the splittings of the second miniband (tight) and the first miniband (loose). This criteria is opposite of what naturally occurs, where the splitting of the upper coupled states is looser than the splitting of lower coupled states. These effects contributed to the slight misalignment of the third miniband, which lies completely in the injector.

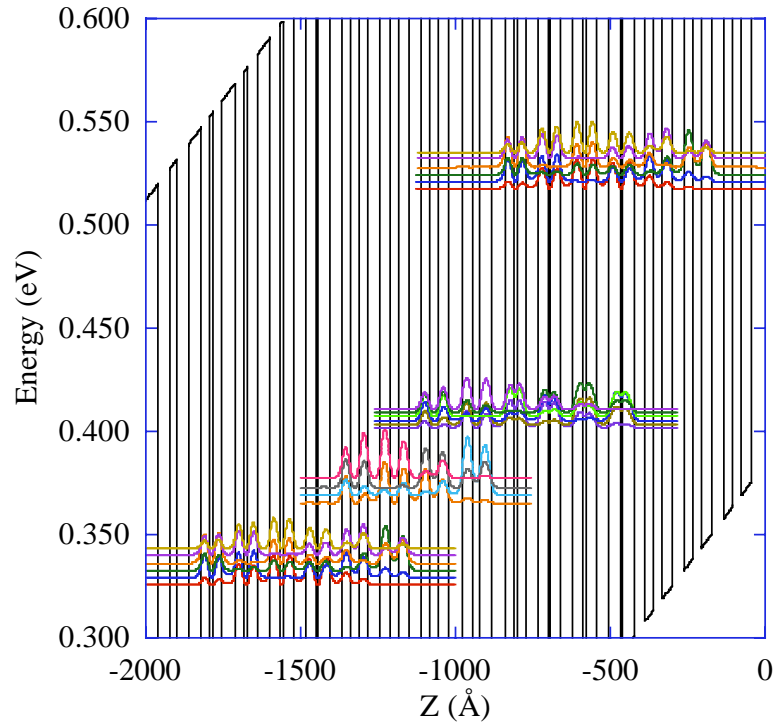


Figure 9: The finished broad gain QCL design.

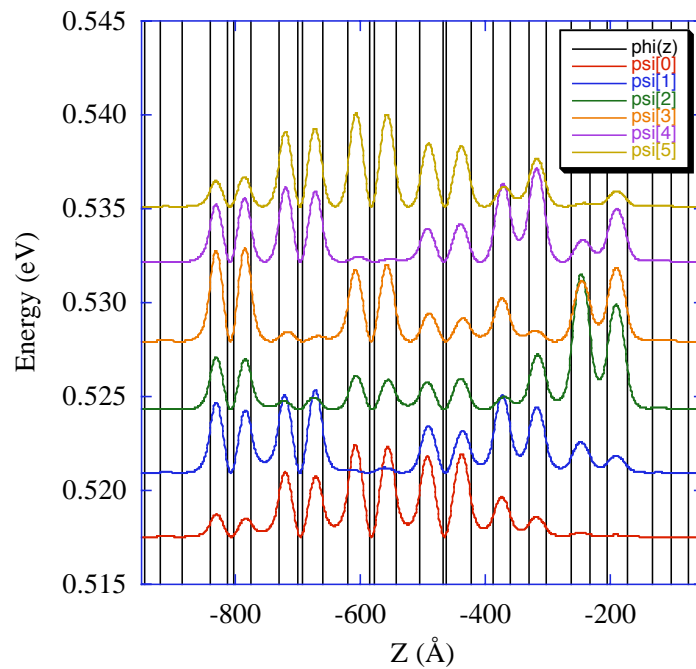


Figure 10: Expanded view of the first (and fourth) miniband in the laser design.

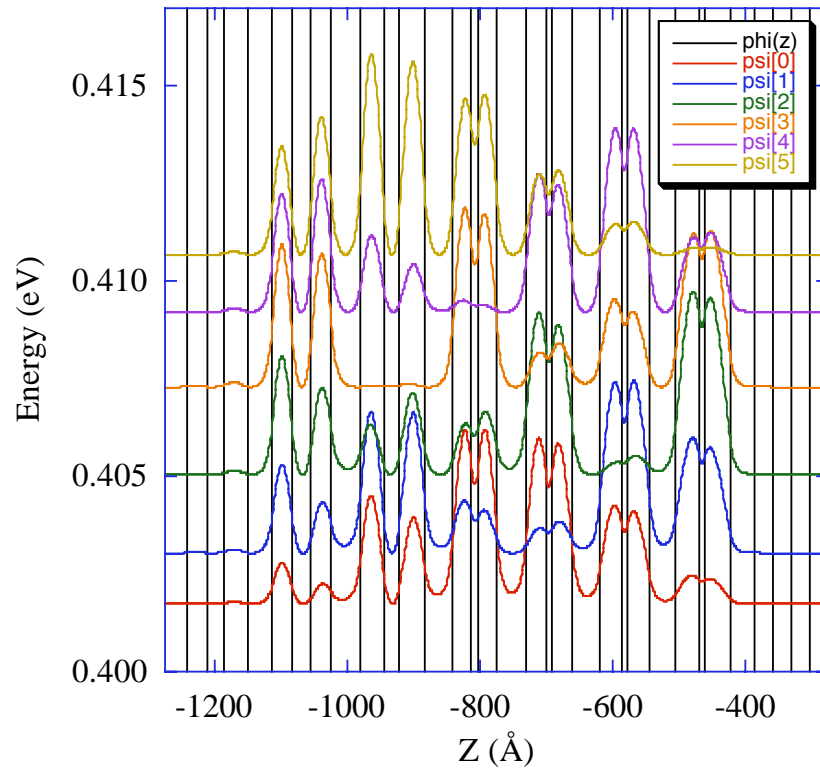


Figure 11: Expanded view of the second miniband in the laser design.

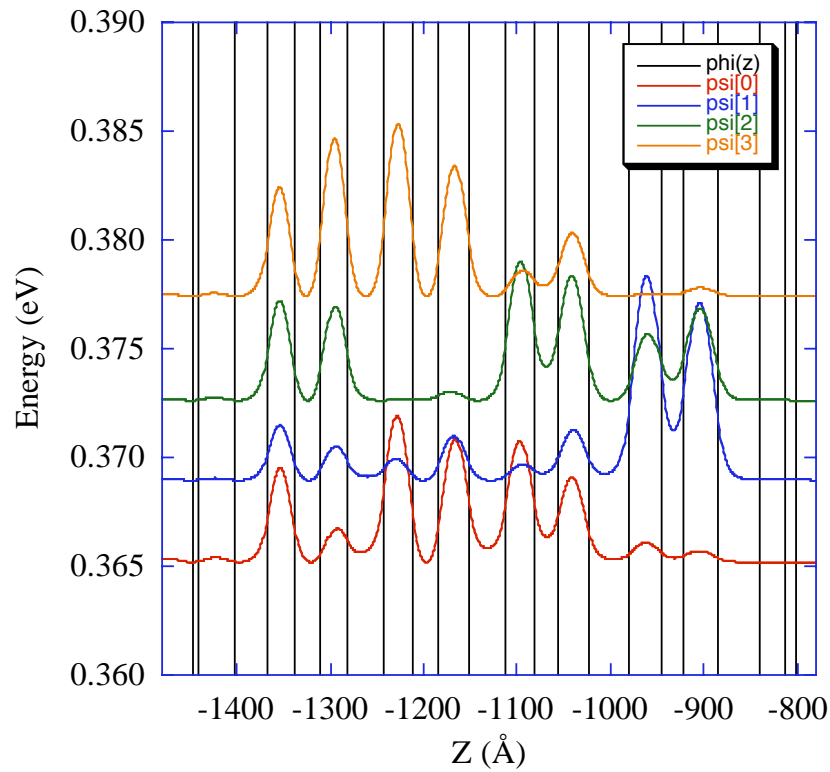


Figure 12: Expanded view of the third miniband in the laser design.

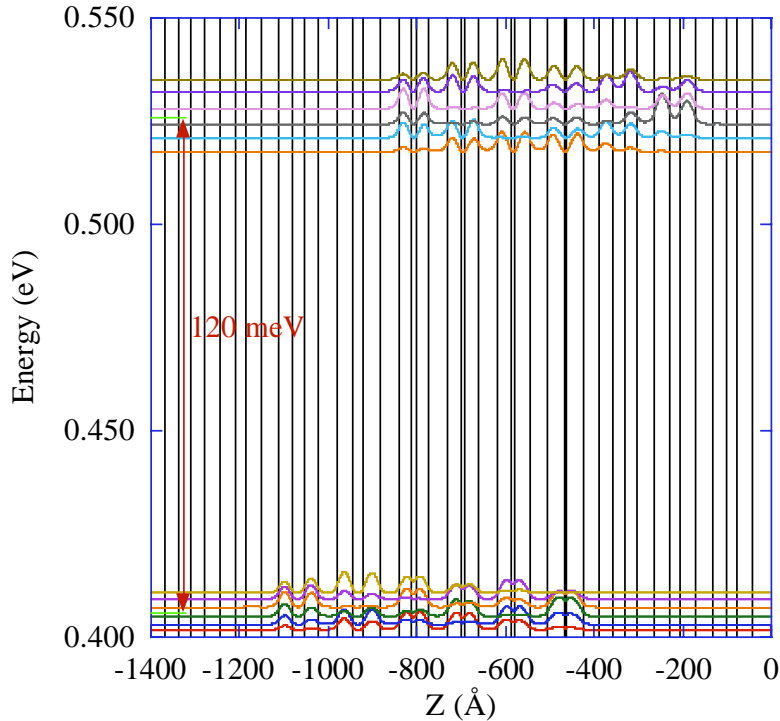


Figure 13: Expanded view of the lasing transition in the laser design.

Expanded views of the three energy drops are shown in Figures 13-15. The lasing transition is shown in Figure 13. The average energy drop between the first and second minibands is exactly 120 meV, the designed energy drop. The first phonon drop is shown in Figure 14, with an average energy drop between the second and third miniband of 35 meV. The second phonon drop is shown in Figure 15, and has an average energy drop between the third and fourth miniband of 37 meV. Both phonon drops were desired to be 36 meV. The slight discrepancy is due to the third miniband being slightly higher than designed. This is attributed to the issues discussed in the preceding paragraph. This should not be of much consequence as most of the individual energy level separations between the two minibands are greater than 36 meV. The combined energy drop of the phonon drops is 72 meV, exactly as designed. The vertical overlap of wavefunctions between each set of minibands is good, allowing for better coupling and between minibands. The coupling strengths are verified by observing that the dipoles between minibands are large.

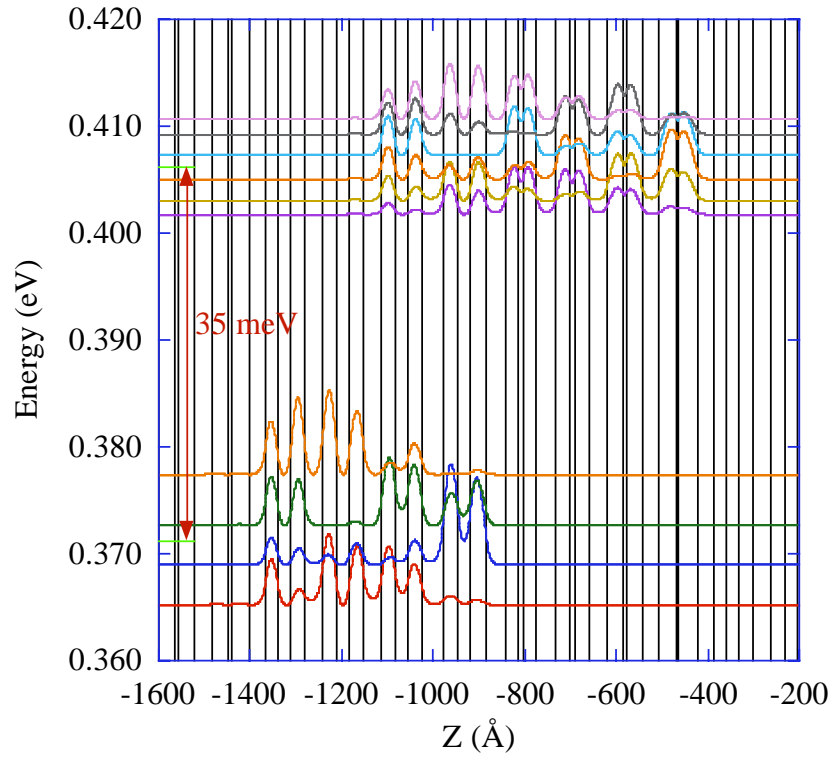


Figure 14: Expanded view of the first phonon drop in the laser design.

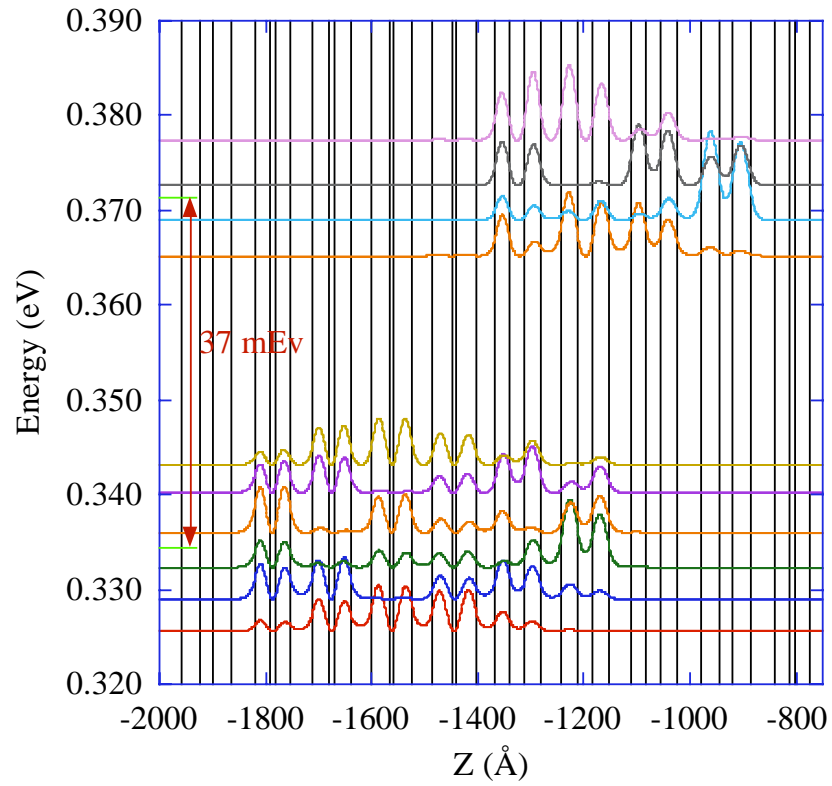


Figure 15: Expanded view of the second phonon drop in the laser design.

3. MEASUREMENTS

Our growth and testing efforts for this project were not quite as successful as our design efforts. Setbacks due to lab moves, growth conditions, and processing were numerous. Other problems were expected, as these are complex structures, and the fundamental basis of our designs had never been tried before. The results of the laser bars and LED's that were fabricated and characterized are described in the following sections.

3.1. First growth

Due to time constraints, Lucent Technologies performed our first round of growths. Two wafers of the original design, D3224 and D3234, were grown. Unfortunately, both samples had very high defect densities, so much so that the surface of the wafer appeared cloudy to the naked eye. Figures 16 and 17 show slightly magnified pictures of the surface of the wafers.

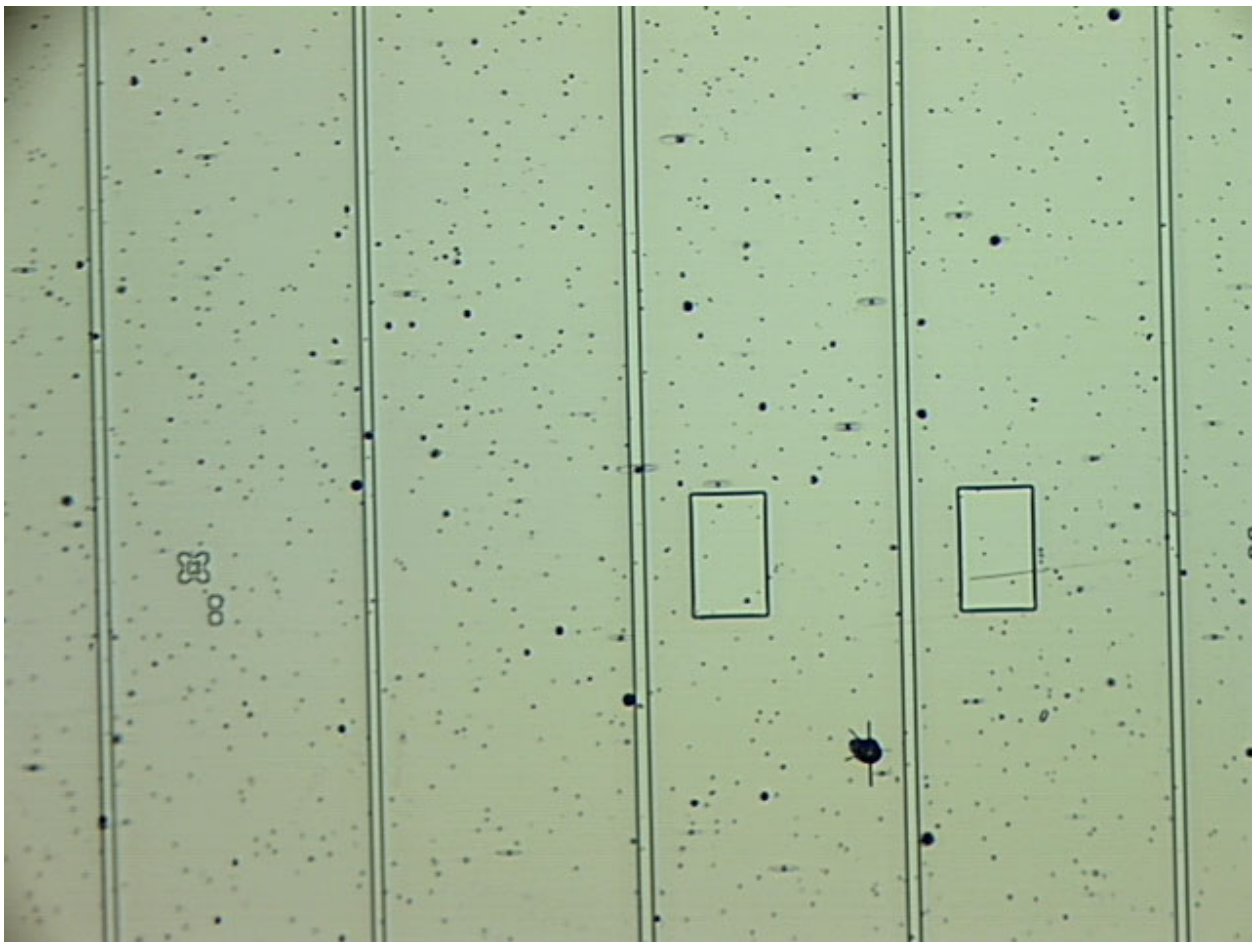


Figure 16: Partly processed sample of D3224 showing the large number of defects. The central waveguide is 24 microns wide.

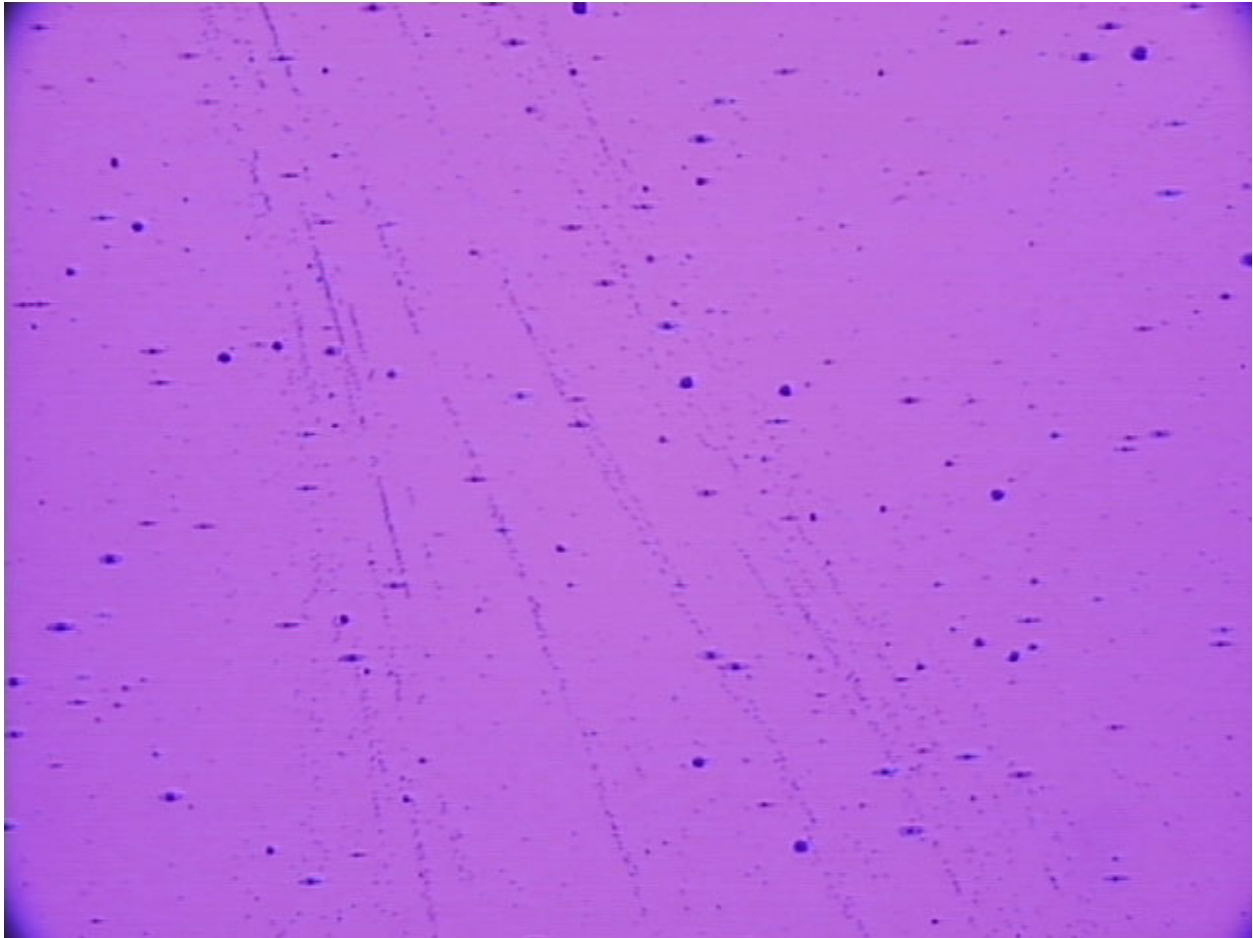


Figure 17: An unprocessed sample of D3234 showing the high defect density.

Laser bars were fabricated from these samples. However, no light was observed. Figure 18 shows a typical current-voltage plot for these samples. A slight kink can be observed at around 4 V. This is the approximate voltage that should give us the designed electric field. However, above this voltage the current should rapidly increase with small increases in voltage resulting in a flat I-V curve, like a diode. Instead, the voltage increases roughly linearly with current, like a resistor. We conclude that the defect density in these devices was too high, causing great losses that prevented lasing.

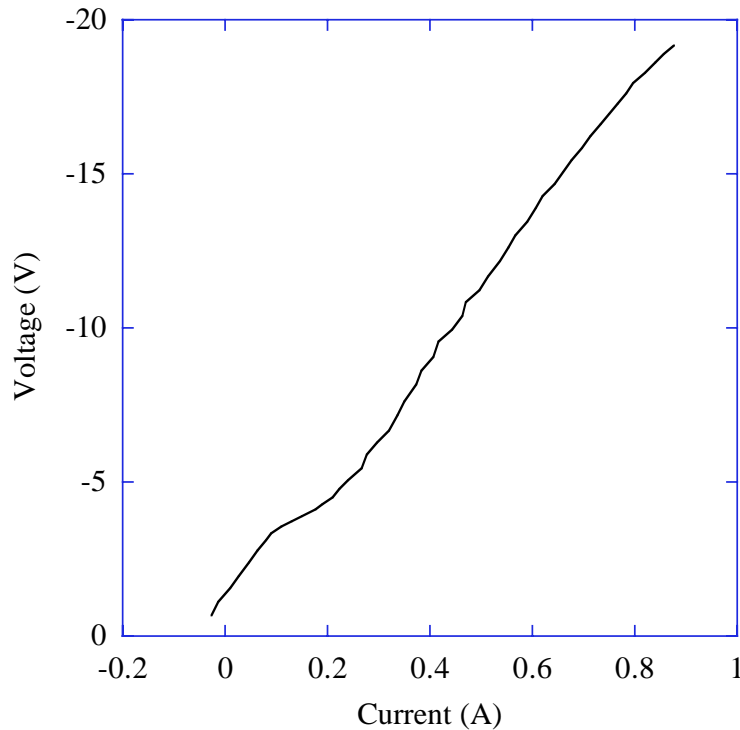


Figure 18: Representative current-voltage plot of laser bars from wafer D3224.

3.2. Second growth

The second round of growth was performed at Sandia. Three wafers were grown: the original design (EB2555), a modified design (EB2571), and a modified design with a factor of 10 higher doping (EB2569) since the current in the original samples was much too low. These wafers were processed into both laser bars and LED's. Initially, no light was observed from either the laser bars or LED's. The lasers showed similar I-V characteristics to that of the first growth. Figure 19 shows a comparison between laser bars from EB2569 and D3224. The slopes of the I-V curves for laser bars from both wafers are nearly the same. However, the location of the bends in the I-V curves for EB2569 occur at about twice the voltage and current of the same features in D3224.

Though no light was observed from the LED's either, critical information was learned. While some of the LED's exhibited poor I-V characteristics (Figures 20, 21), others had the type of I-V characteristics that one would expect of a miniband quantum cascade laser. Figure 22 shows the current-voltage curve of an LED of the original design (EB2555). The diode characteristics can easily be seen, with the knee of the curve occurring at 4V. At a bias of 6.7V, 1A for the diode cooled to 4K, the voltage jumps sharply and begins a series of small jumps, all at a greater slope than before. This is due to states of the miniband snapping out of place. A similar behavior is seen at room temperature operation. The I-V curves suggest that the current transport is behaving as designed, even if the devices do not emit light.

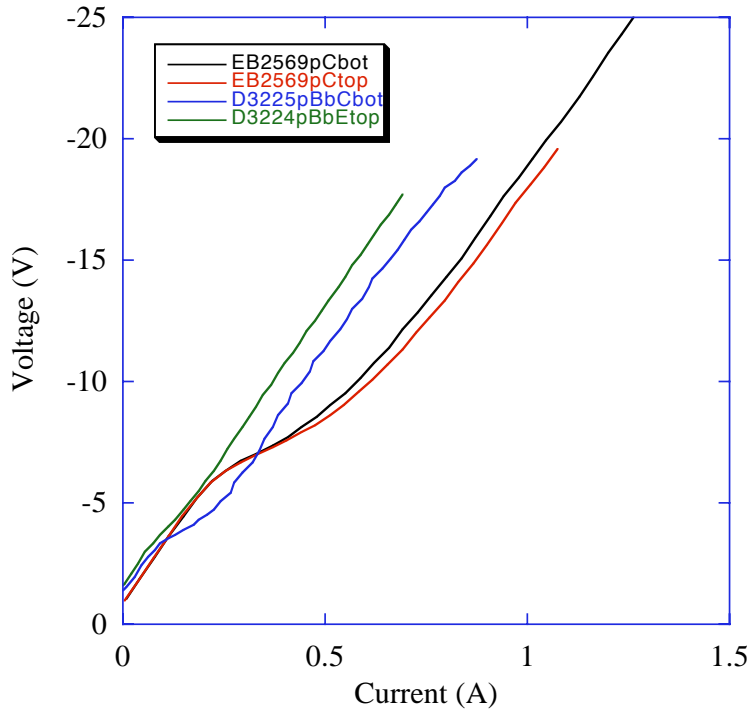


Figure 19: Comparison of current-voltage curves for laser bars from EB2569 and D3224.

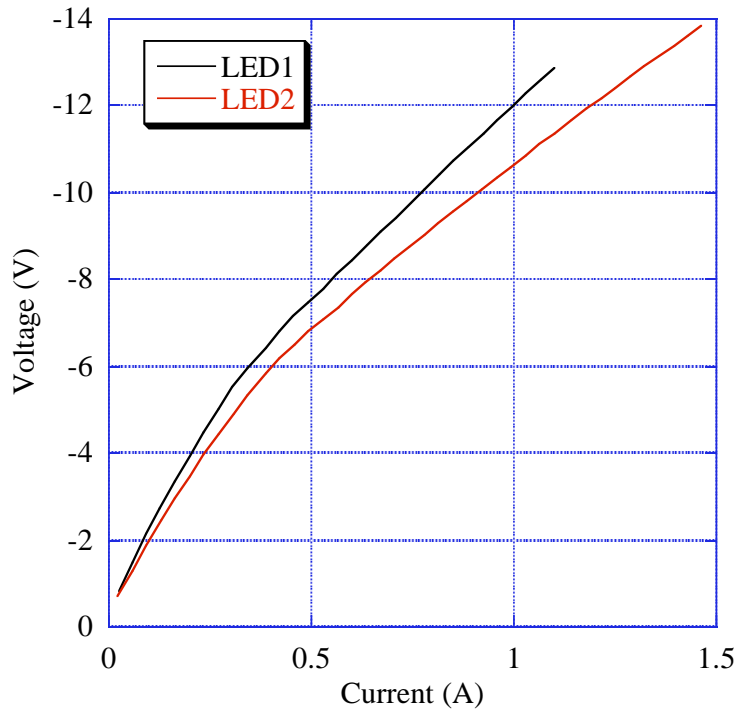


Figure 20: Current-voltage curves at $T = 4K$ for two LED's fabricated from wafer EB2569.

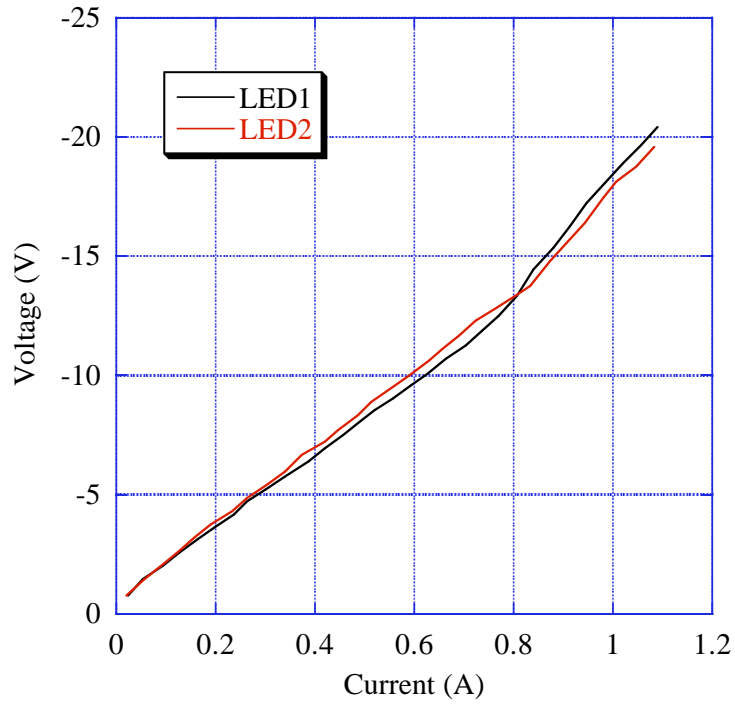


Figure 21: Current-voltage curves at $T = 294\text{K}$ for LED's fabricated from wafer EB2571.

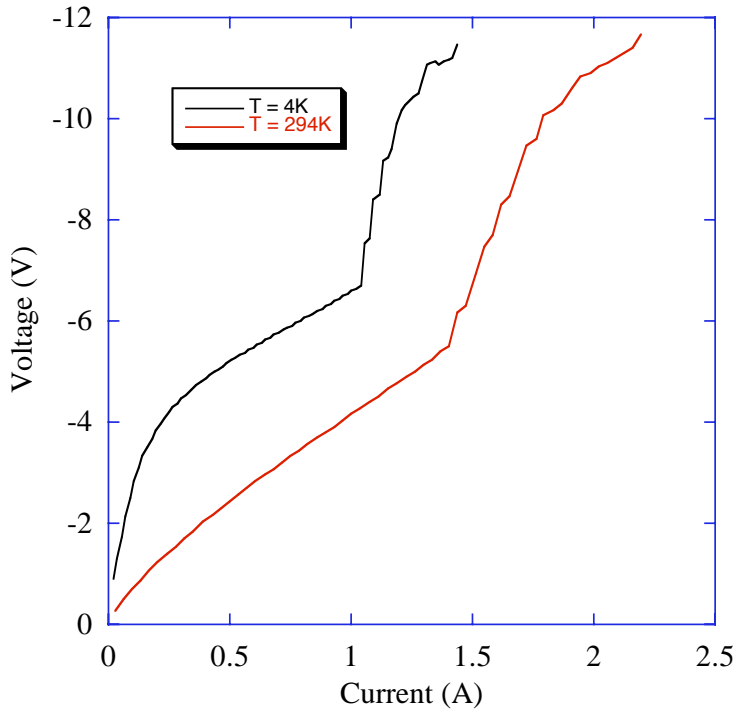


Figure 22: Current-voltage curves at $T=4\text{K}$ and $T=300\text{K}$ for an LED from wafer EB2555.

Performing measurements of light emitted from these devices is tricky. The I-V characteristics of Figure 22 suggest that light should be emitted. However, the amount of light from these LED's is expected to be extremely small, in the microwatt range. Furthermore, since the design wavelength is 10 microns, there is no available IR card to do a quick check for the presence of light. Complicating the issue is the fact that the sample must be cooled to cryogenic temperatures for proper operation. During the measurements, the samples were placed in a continuous flow cryostat cooled with liquid helium. This made proper alignment between the detector and LED difficult to verify. The light from the laser bars should have been more powerful, in the milliwatt range if they lased, and thus easy to detect and align to, yet none was observed.

The absence of laser light and the differences between the I-V curves of the lasers and LED's is consistent with a large defect density. The areas of the two types of devices are different. The processed laser bars typically are 20 microns wide and 3 mm long, resulting in a surface area of 60000 square microns. The fabricated LED's are round mesas 200 microns in diameter, having a surface area of roughly 31,400 square microns, or half the area of the laser bars. Thus we expected similar IV's except that the current in the laser should have been twice as large as in the LED.

The LED's degrade over time. Figure 23 shows current-voltage curves measured on three different days. For each set of measurements, the devices must be cooled down from room temperature to 4K. After the measurements are complete, the devices are brought back to room temperature. This temperature cycling could help contribute to the propagation of defects. Another source of degradation could be aging due to current injection. It is possible that the defects propagate as carriers are pushed through the structure.

Recently, colleagues at Princeton have observed lasing from the highly doped sample, EB2569. However, as shown in Figure 24, the lasing wavelength was 1.58 microns, not the design wavelength. The laser light had almost equal strength in both polarizations. These facts point towards the laser being an interband laser, since the photon energy is comparable to the material bandgap, and much larger than the energy level separations allowed in the material system chosen and the fact that QC lasers only emit TM polarized light. We postulate that somewhere in the laser a p-n junction has formed. The dopant used in the growth is Si, which is a group IV element and thus amphoteric. It is possible that the Si dopants replaced As sites instead of any of the group III sites, resulting in p-type doping instead of n-type.

Our colleagues at Princeton also observed light emission from a laser bar from sample EB2571. A Ge lens was used to filter out any emissions in the near-IR regime. A signal peak was observed at 1250 cm^{-1} (Figure 25), which corresponds to a wavelength of 8 microns. This means the transition energy is 155 meV, exactly the average energy drop between the first and third minibands (Figures 13 and 14). However, examination of the dipoles between these minibands shows that direct energy transitions between these two minibands are unlikely. It is possible that impurity states populated through carrier freeze-out are lowering the ground states of the wells, enabling a larger energy drop between the first and second minibands that serendipitously is 155 meV.

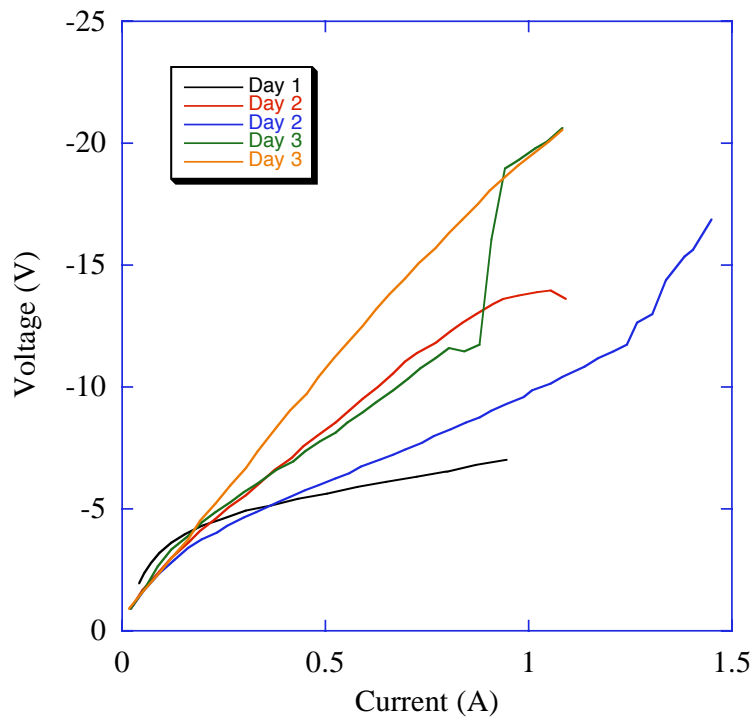


Figure 23: Degradation of the current-voltage curve over time of and LED from wafer EB2555.

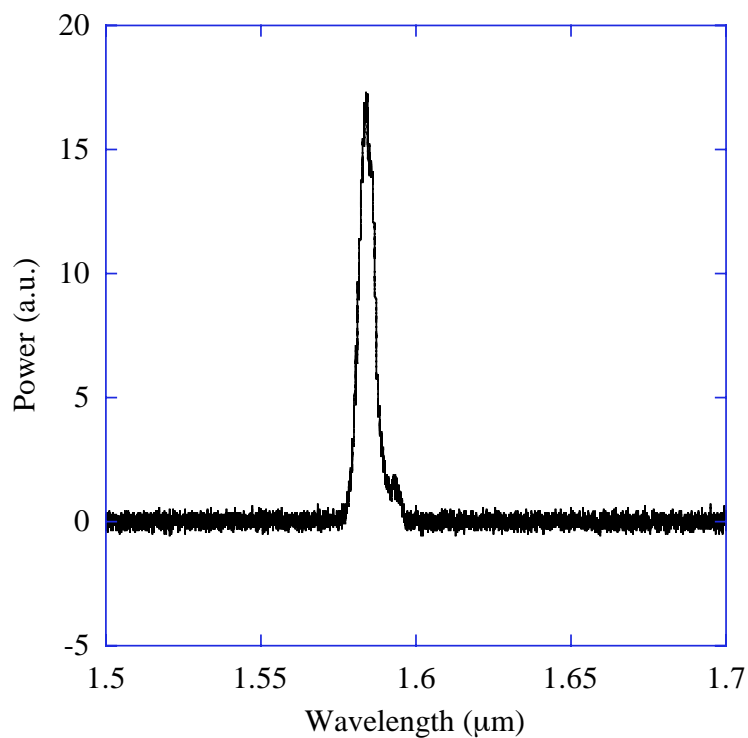


Figure 24: Spectrum of lasing sample from EB2569.

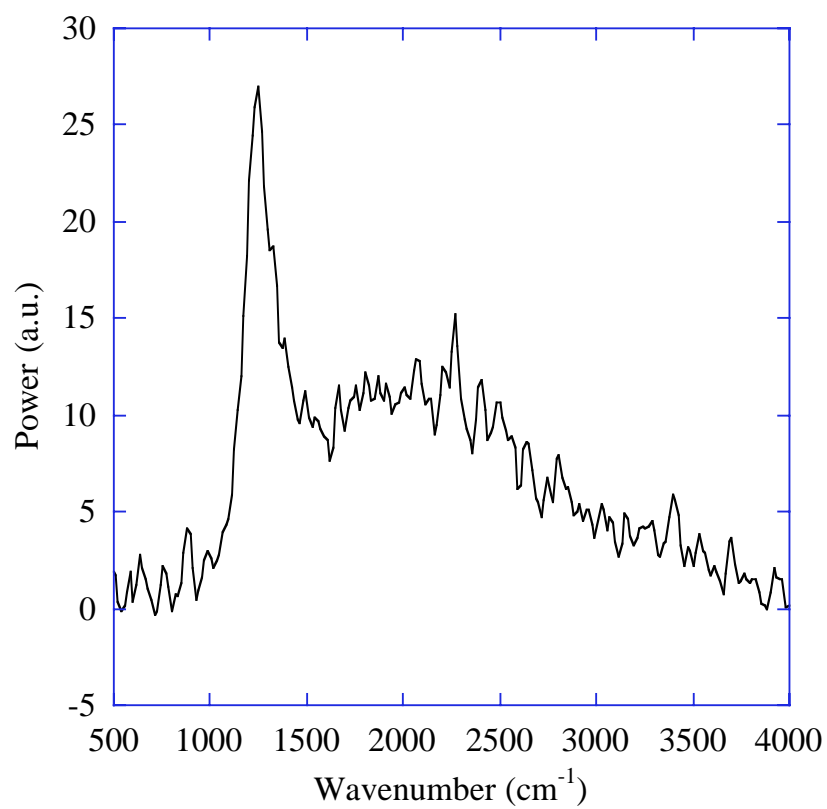


Figure 25: Spectrum of light emission from EB2571.

4. CONCLUSIONS

We have successfully developed automated design software that can quickly and efficiently produce a quantum cascade laser design given the necessary input criteria. By specifying the size of the energy drops and the amount of splitting between matched energy levels, miniband-to-miniband quantum cascade lasers can now be designed in minutes, rather than days or weeks. The code is modular and easily reconfigurable to allow for the design of any type of quantum cascade laser. Our group, and by extension Sandia, now has the tools to reduce turnaround time and improve consistency between quantum cascade laser designs, as well as provide enhanced, quick, and economical designs of a variety of quantum cascade lasers.

We have grown, characterized, and iterated designs of miniband-to-miniband quantum cascade lasers. Though we have yet to observe lasing at the design frequency, the I-V curves of LED's from the original design show that the minibands are forming as predicted. Lasing is expected once the growth, processing, and doping issues are more fully understood and resolved.

As with all good LDRD projects, the risks involved were high. Though not all of the desired goals were met, there was success. We have gained a greater understanding of the principles of broad gain quantum cascade lasers as well as enhanced our design software, both of which will prepare us for future success.

APPENDIX A: PROGRAM CODE

```
% WBG13 Make the wbg13 structure.
% WBG13 is a standalone program that produces the wbg13 structure.
% The program is a duplicate of STRUCTBUILDerv3 with the proper inputs to
% produce the wbg13 structure.
%
% See also STRUCTBUILDerv3, WBG14INJONLY.

% by Erik Young

clear all
close all
format short

%%%%%%%%%% inputs %%%%%%%%%%%
defaultstructfilepath= ... %enter location of default structure file
    '/Users/ewyoung/Desktop/QCwavefunctionCode/Structures/';
feedback=0;
flat=1;
fieldfudge=0; %field fudge factor, old: 0.0014
matchtol=0.0001 %tolerance on cell match, in eV
levelcond=0.00001; %band flatness, in Angstroms
lockedin=1; %chooses whether to iterate on first try

%%%%%% first well %%%%
bandgap=0.120; %desired bandgap in eV
bandgaptol=0.0001; %bandgap accuracy in eV
initfield=19.5984; %initial guess for the E-field (kV/cm)
barwidth=5.8697; %width of first well barrier
%%%%%%%%%%

%%%%%% activereg %%%%
numwells=4; %number of bi-wells in active region
trgtsplit=0.01; %desired band2 splitting in eV
splitcond=0.0001; %desired split accuracy in eV
b2cond=0.01;
b1cond=0.01;
origstep2=1; %inital step size, band2, in Angstroms
origstep1=0.5; %inital step size, band1, in Angstroms
%%%%%%%%%%
```

```

%%%% injector %%%%%
injd1trgtsplit=0.005;      %desired band2 splitting in eV
injd1splitcond=0.0001;   %desired split accuracy in eV
injd1b2cond=0.01;
injd1b1b2trgtsplit=0.036; %desired b1-b2 splitting in eV
injd1b1b2splitcond=0.0001; %desired b1-b2 split accuracy in eV
injd1origstep2=1;        %inital step size, band2, in Angstroms
injd1origstep1=0.5;      %inital step size, band1, in Angstroms

injm1numwells=2;         %number of bi-wells in active region
injm1trgtsplit=0.0057;   %desired band2 splitting in eV
injm1splitcond=0.0001;   %desired split accuracy in eV
injm1b2cond=0.01;
injm1b1cond=0.01;
injm1origstep2=1;        %inital step size, band2, in Angstroms
injm1origstep1=0.5;      %inital step size, band1, in Angstroms

injd2trgtsplit=0.0075;   %desired band2 splitting in eV
injd2splitcond=0.0001;   %desired split accuracy in eV
injd2b2cond=0.01;
injd2b1b2trgtsplit=0.036; %desired b1-b2 splitting in eV
injd2b1b2splitcond=0.0001; %desired b1-b2 split accuracy in eV
injd2origstep2=1;        %inital step size, band2, in Angstroms
injd2origstep1=0.5;      %inital step size, band1, in Angstroms

injm2numwells=2;         %number of bi-wells in active region
injm2trgtsplit=0.0093;   %desired band2 splitting in eV
injm2splitcond=0.0001;   %desired split accuracy in eV
injm2b2cond=0.01;
injm2b1cond=0.01;
injm2origstep2=1;        %inital step size, band2, in Angstroms
injm2origstep1=0.5;      %inital step size, band1, in Angstroms

injd3trgtsplit=trgtsplit; %desired band2 splitting in eV
injd3splitcond=0.0001;   %desired split accuracy in eV
injd3b2cond=0.01;
injd3b1b2trgtsplit=bandgap; %desired b1-b2 splitting in eV
injd3b1b2splitcond=bandgaptol; %desired b1-b2 split accuracy in eV
injd3origstep2=1;        %inital step size, band2, in Angstroms
injd3origstep1=0.5;      %inital step size, band1, in Angstroms
%%%%%%

```

```

%%%%%%%%

```

```

%%%% Set up file names %%%
DSF=importdata(strcat(defaultstructfilepath,'DefaultStructureFile'), 't'); %read in default
structure file
structfilename=strcat(defaultstructfilepath,char(DSF(2)),',',char(DSF(1))); %make full path
plotfilename=strcat(structfilename,'_WFNs.txt');
energyfilename=strcat(structfilename,'_EDL.txt');
actstructfilename=strcat(structfilename,'_active');
injstructfilename=strcat(structfilename,'_injector');
%%%%%%%%%%%%%%%%%%%%%%%%%%%%%%%%%%%%%%%%%%%%%%%%%%%%%%%%%%%%%%%%%%%%%%%%

desdrop=bandgap+injd1b1b2trgtsplit+injd2b1b2trgtsplit; %in eV
field=initfield;
count=0;
flatbak=flat;           %save flatness choice
if lockedin==0
    flat=0;             %initially set to 0, regardless
    lastbarflag=0;     %initialize to 0
    barflagcount=0;    %initialize to 0
else
    lastbarflag=1;     %iterate final barrier
    barflagcount=1;    %set on first loop
end

banddrop=desdrop;
drop=banddrop+2*matchtol; %garbage to make loop work 1st time
match=drop-banddrop;

%%%%%%%%%% Big Loop %%%%%%%%%%
while abs(match)>matchtol
count=count+1;
states=0;           %counter for # of designed states

%%%%%%%%%% Determine Field %%%%%%%%%%
if (drop>banddrop)&(count>1) %field is too high
    newfield(count)=(banddrop/thickness)*1e5*(1-fieldfudge); %in kV/cm
    field=newfield(count);
elseif (drop<banddrop)&(count>1) %field is too low
    newfield(count)=(banddrop/thickness)*1e5*(1+fieldfudge); %in kV/cm
    field=newfield(count);
else %count=1
    newfield(1)=field;
end

```

```

if (lastbarflag==0)&(count>(barflagcount+3))
    newfield(count)=(newfield(count)+newfield(count-1))/2;
    field=newfield(count);
end

if (lastbarflag==1)&(count>(barflagcount+2))
    newfield(count)=(newfield(count)+newfield(count-1))/2;
    field=newfield(count);
end

%%%%%%%%%%%%%%%%%%%%%%%%%%%%%%%%%%%%%%%%%%%%%%%%%%%%%%%%%%%%%%%%%%%%%%%%

firstwellv3(structfilename, bandgap, bandgaptol, field, barwidth, flat, levelcond);
states=states+2;
wavefxnplot(plotfilename)      %plot first well wavefunctions

activereg2(structfilename, numwells, trgtsplit, splitcond,...
    b2cond, b1cond, origstep2, origstep1, feedback, flat, levelcond);
states=states+2*numwells-2;
wavefxnplot(plotfilename)      %plot active region wavefunctions

%%%%%%%%%%%%%%%%%%%%%%%%%%%%%%%%%%%%%%%%%%%%%%%%%%%%%%%%%%%%%%%%%%%%%%%% Save Active Region, prepare structure file %%%%%%%%%%%
C=importdata(structfilename, '\t'); %read in file
changestruct(actstructfilename, 0, 0, C); %copy struct to active file
C=shuffle(structfilename, 2);      %prepare structure file
%%%%%%%%%%%%%%%%%%%%%%%%%%%%%%%%%%%%%%%%%%%%%%%%%%%%%%%%%%%%%%%%%%%%%%%%

injectorv2(structfilename, injd1trgtsplit, injd1splitcond,...
    injd1b2cond, injd1b1b2trgtsplit, injd1b1b2splitcond,...
    injd1origstep2, injd1origstep1, feedback, flat, levelcond)
states=states+2;
wavefxnplot(plotfilename)      %plot first injector drop

%%%%%%%%%%%%%%%%%%%%%%%%%%%%%%%%%%%%%%%%%%%%%%%%%%%%%%%%%%%%%%%%%%%%%%%% store and set up injector file %%%%%%%%%%%
C=shuffle(structfilename, 1);      %prepare structure file
C.data(1,:)=C.data(5,:);          %move barrier
C.textdata=C.textdata(1:5);      %keep only first well
C.data=C.data(1:4,:);            %keep only first well
changestruct(injstructfilename, 0, 0, C); %copy struct to injector file
%%%%%%%%%%%%%%%%%%%%%%%%%%%%%%%%%%%%%%%%%%%%%%%%%%%%%%%%%%%%%%%%%%%%%%%%

activereg2(structfilename, injm1numwells, injm1trgtsplit, injm1splitcond,...
    injm1b2cond, injm1b1cond, injm1origstep2, injm1origstep1, feedback,...
    flat, levelcond);
states=states+2*injm1numwells-2;
wavefxnplot(plotfilename)      %plot first injector match

```

```

%%%%%%%% update injector file, prep struc file %%%%%%%%%
C=shuffle(structfilename, 1); %prepare structure file
D.textdata=C.textdata(5:9); %copy last four layers
D.data=C.data(5:8,:); %copy last four layers
changestruct(injstructfilename, 0, 0, D, 'a'); %copy struct to injector file
%%%%%%%%

```

```

injectorv2(structfilename, injd2trgtsplit, injd2splitcond,...
    injd2b2cond, injd2b1b2trgtsplit, injd2b1b2splitcond,...
    injd2origstep2, injd2origstep1, feedback, flat, levelcond)
states=states+2;
wavefxnplot(plotfilename) %plot second injector drop

```

```

%%%%%%%% update injector file %%%%%%%%%
C=shuffle(structfilename, 1); %prepare structure file
D.textdata=C.textdata(5:9); %copy last four layers
D.data=C.data(5:8,:); %copy last four layers
changestruct(injstructfilename, 0, 0, D, 'a'); %copy struct to injector file
%%%%%%%%

```

```

activeregv2(structfilename, injm2numwells, injm2trgtsplit, injm2splitcond,...
    injm2b2cond, injm2b1cond, injm2origstep2, injm2origstep1, feedback,...
    flat, levelcond);
states=states+2*injm2numwells-2;
wavefxnplot(plotfilename) %plot second injector match

```

```

%%%%%%%% update injector file %%%%%%%%%
C=importdata(structfilename, '\t'); %read in file
C.textdata(2:5)=C.textdata(6:9); %copy last four layers
C.data(1:4,:)=C.data(5:8,:); %copy last four layers
C.textdata=C.textdata(1:5); %keep only first well
C.data=C.data(1:4,:); %keep only first well
changestruct(injstructfilename, 0, 0, C, 'a'); %copy struct to injector file
%%%%%%%%

```

```

C=importdata(injstructfilename, '\t'); %read in file
changestruct(structfilename, 0, 0, C); %rewrite structure file
tryit3; %call QC program
wavefxnplot(plotfilename) %plot injector wavefunctions

```

```

%% %% estimate width of last(first) barrier %% %%
if lastbarflag==1
    C=importdata(injstructfilename, '\t'); %read in structure file
    D=importdata(actstructfilename, '\t'); %read in active region file
    sz=size(C.data,1);
    C.textdata(3:5)=C.textdata((sz-1):sz+1); %keep last three layers
    C.data(2:4,:)=C.data((sz-2):sz,:); %keep last three layers
    C.textdata(6)=C.textdata(sz-2); %copy barrier
    C.data(5,:)=C.data(sz-3,:); %previous barrier is initial barrier guess
    C.textdata=C.textdata(1:6); %keep only first well & barrier
    C.data=C.data(1:5,:); %keep only first well & barrier
    C.textdata(2)=D.textdata(2); %copy barrier
    C.data(1,:)=D.data(1,:); %copy barrier
    C.textdata(7:9)=D.textdata(3:5); %copy first well of active region
    C.data(6:8,:)=D.data(2:4,:); %copy first well of active region
    changestruct(structfilename, 0, 0, C); %rewrite structure file
    injectorv1b(structfilename, injd3trgtsplit, injd3splitcond,...
        injd3b2cond, injd3b1b2trgtsplit, injd3b1b2splitcond,...
        injd3origstep2, injd3origstep1, feedback)
    wavefxnplot(plotfilename) %plot second injector drop
end
%% %% %% %% %% %% %% %% %% %% %% %% %% %% %% %% %% %% %% %% %% %% %% %% %% %% %% %% %%

%% %% %% %% %% %% update files %% %% %% %% %%
D=importdata(structfilename, '\t'); %read in file
C=importdata(actstructfilename, '\t'); %read in file
C.data(1,:)=D.data(5,:); %replace initial barrier
changestruct(actstructfilename, 0, 0, C); %rewrite active region file
changestruct(structfilename, 0, 0, C); %rewrite structure file
C=importdata(injstructfilename, '\t'); %read in file
changestruct(structfilename, 0, 0, C, 'a'); %add to structure file
C=importdata(structfilename, '\t'); %read in file
C.data
tryit3; %call QC program
wavefxnplot(plotfilename) %plot injector wavefunctions
%% %% %% %% %% %% %% %% %% %% %% %% %% %% %% %% %% %% %% %% %% %% %% %% %%

```



```

%%%%%%%%%% determine drop %%%%%%%%%%%
y=dlmread(plotfilename, '\t', 1, 0); %read wfxn data, skip headers
banddrop= (sum(y(1,((states+3)-3):(states+3)))/4)-(sum(y(1,4:5))/2) %in eV
% banddrop= (sum(y(1,16:19))/4)-(sum(y(1,4:5))/2) %in eV
C=importdata(structfilename, '\t'); %read in file
thickness=sum(C.data(:,2)) %in Angstroms
drop=thickness*field/1e5 %in eV
match=drop-banddrop
states
count
newfield
%%%%%%%%%%

%%%%%%%%%% set flags %%%%%%%%%%%
if ((abs(match)<=matchtol)|(count>1))&(lastbarflag==0)
    lastbarflag=1; %calculate last barrier
    flat=flatbak; %use original flatness choice
    barflagcount=count; %count at which lastbarflag was set
    match=2*matchtol; %run the Big Loop again
end
%%%%%%%%%%

end
%%%%%%%%%% End Big Loop %%%%%%%%%%%
tryit3anal; %call QC program with analysis

```

DISTRIBUTION

1	MS1071	Jay Jakubczak	5710
1	MS1071	Andy Boye	1720
1	MS0980	Tom Zipperian	1740
1	MS1079	Gil Herrera	1700
1	MS1082	Erik Young	1725
1	MS1082	Mike Wanke	1725
1	MS1082	Chuck Fuller	1725
1	MS1082	Sally Samora	1725
1	MS1082	Jim Hudgens	1725
1	MS1085	John Klem	1742
1	MS1085	Charles Sullivan	1742
2	MS9018	Central Technical Files	8944
2	MS0899	Technical Library	4536
1	MS0161	Patent and Licensing Office	11500
1	MS0123	Donna Chavez, LDRD Office	1011